An Introduction to the Winfrith Concrete Model

Len Schwer
Schwer Engineering & Consulting Services
Len@Schwer.net

April 2010

Introduction

The so called Winfrith concrete model in LS-DYNA (MAT084 and MAT085) provides:

- A basic plasticity model that includes the third stress invariant for consistently treating both triaxial compression and triaxial extension, e.g. Mohr-Coulomb like behavior,
- Uses radial return which omits material dilation, and thus violates Drucker's Postulate for a stable material,
- Includes strain softening in tension with an attempt at regularization via crack opening width, fracture energy, and aggregate size,
- Optional strain rate effects: MAT084 includes rate effects and MAT085 does not,
- Concrete tensile cracking with up to three orthogonal crack planes per element; crack viewing is also possible via an auxiliary post-processing file,
- Optional inclusion of so called 'smeared reinforcement.'

In this introductory document only the basic plasticity model will be described. This description will allow for the determination of which portions of a model have reached the shear failure surface. Additionally, comparison of the shear failure surface of the *MAT_WINFRITH_CONCRETE model with other so called 'simple input' concrete models, e.g., *MAT_PSEUDO_TENSOR (MAT016), *MAT_CONCRETE_DAMAGE_REL3 (MAT072R3) and *MAT_CSCM_CONCRETE (MAT159), will be possible.

A note on sign convention: in geomechanics compression is usually considered as positive, since most stress states of interest are compressive. However, the Winfrith model uses the standard engineering mechanics convention of compression as negative.

Ottosen Plasticity Model

The plasticity portion of the Winfrith concrete model is based upon the shear failure surface proposed by Ottosen (1977):

$$F\left(I_1, J_2, \cos 3\theta\right) = a\frac{J_2}{\left(f_c'\right)^2} + \lambda\frac{\sqrt{J_2}}{f_c'} + b\frac{I_1}{f_c'} - 1 \tag{1}$$

The above is referred to as a four parameter model: the constants a and b which control the meridional shape of the shear failure surface, and $\lambda = \lambda\left(\cos 3\theta\right)$ ranging $-1 \le \cos 3\theta \le +1$ for triaxial compression to triaxial extension control the shape of the shear failure surface on the π-plane. In addition to an explicit dependence on the unconfined compressive strength, f_c', as will be demonstrated, the constants a and b also depend on the ratio of the unconfined *tensile* strength, f_t', to the unconfined compressive strength.

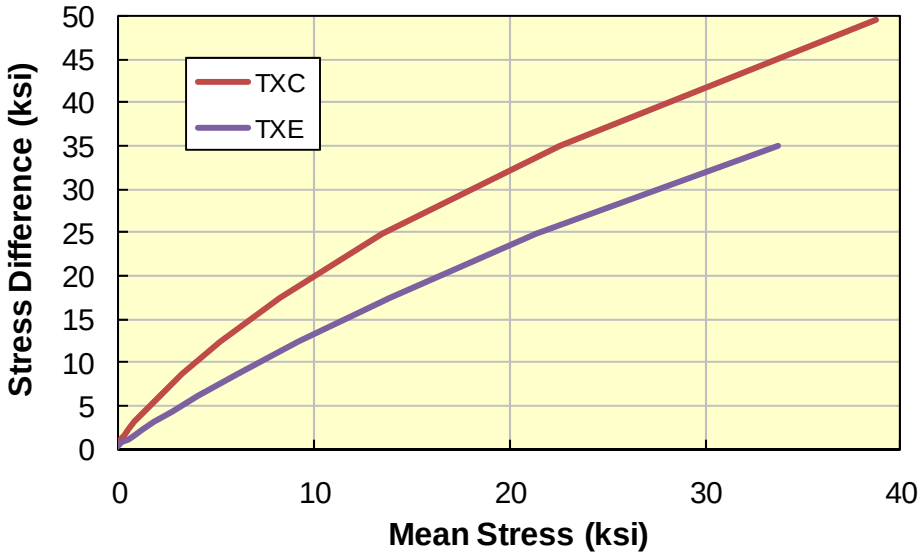

Figure 1 Illustration of Ottosen shear failure surfaces for a 6 ksi unconfined compression strength concrete.

One oddity of the Ottosen shear failure surface is it is both a function J_2 and $\sqrt{J_2}$ unlike almost all other geomaterial shear failure surfaces which are only functions of $\sqrt{J_2}$. This makes plotting traditional view of the shear failure surface in $\left(I_1, \sqrt{J_2}\right)$ space, or alternatively (mean stress, stress difference), a bit different. However, noting Equation (1) is quadratic in the ratio $\sqrt{J_2} / f_c'$ allows for the alternative form of

$$\begin{aligned} \frac{\sqrt{J_2}}{f_c'} &= \frac{-B+\sqrt{B^2-4AC}}{2A} \\ A &= a \\ B &= \lambda \\ C &= b\frac{I_1}{f_c'}-1 \end{aligned} \tag{2}$$

Thus once the parameters a, b, and λ are determined the independent parameter I_1 can be varied to generate the triaxial compression and extension surfaces. Figure 1 shows the triaxial compression $\left(\sigma_1 > \sigma_2 = \sigma_3\right)$ and triaxial extension $\left(\sigma_2 = \sigma_3 > \sigma_1\right)$ surfaces for an f_c'=6 ksi (41 MPa) concrete.

Stress Invariants

To be consistent with the source coding of the Winfrith model, first the invariants of the stress tensor are calculated and then using identities the required invariants of the deviatoric stress tensor are computed.

The stress tensor, σ_{ij} , is assume to be symmetric with six components:

$$\boldsymbol{\sigma} = \sigma_{ij} = \begin{bmatrix} \sigma_{11} & \sigma_{12} & \sigma_{31} \\ \sigma_{12} & \sigma_{22} & \sigma_{23} \\ \sigma_{31} & \sigma_{23} & \sigma_{33} \end{bmatrix} \tag{3}$$

All third order tensors have three scalar invariants (Eigenvalues), for the stress tensor these are[1]

$$\begin{aligned} I_1 &= \sigma_{kk} = \sigma_{11} + \sigma_{22} + \sigma_{33} \\ I_2 &= 0.5\left(\sigma_{ii}\sigma_{jj} - \sigma_{ij}\sigma_{ji}\right) \\ &= \sigma_{11}\sigma_{22} + \sigma_{22}\sigma_{33} + \sigma_{33}\sigma_{11} - \sigma_{12}^2 - \sigma_{23}^2 - \sigma_{31}^2 \\ I_3 &= DET\left(\sigma_{ij}\right) \\ &= \sigma_{11}\sigma_{22}\sigma_{33} + 2\sigma_{12}\sigma_{23}\sigma_{31} - \sigma_{12}^2\sigma_{33} - \sigma_{23}^2\sigma_{11} - \sigma_{13}^2\sigma_{22} \end{aligned} \tag{4}$$

In constitutive modeling it is often convenient to separate the mean stress (pressure) from the shear response. This is accomplished by introducing the deviatoric stress tensor S_{ij}

$$S_{ij} = \sigma_{ij} - \frac{\sigma_{kk}}{3} \tag{5}$$

Where $\sigma_{kk} = I_1 = 3P$ and P is usually referred to as the mean stress; if all three components of the mean stress are equal then it is referred to as the pressure.

The invariants of the deviatoric stress tensor are related to the stress invariants via the following identities:

$$\begin{aligned} J_1 &= S_{kk} = S_{11} + S_{22} + S_{33} = 0 \\ J_2 &= 0.5 S_{ij} S_{ij} = \frac{1}{3} I_1^2 - I_2 \\ J_3 &= DET\left(S_{ij}\right) = \frac{2}{27} I_1^3 - \frac{1}{3} I_1 I_2 + I_3 \end{aligned} \tag{6}$$

[1] See for example http://en.wikipedia.org/wiki/Stress_(mechanics)

Often in the continuum mechanics literature the notation J_2' and J_3' are used with the superscript prime reinforcing the deviatoric stress aspect of the invariants. The third deviatoric stress invariant is rarely used directly, rather a geometric interpretation as an angle in the π-plane with limits $0 \le \theta < \frac{\pi}{3}$ is defined by

$$\cos 3\theta = \frac{3\sqrt{3}}{2} \frac{J_3}{J_2^{1.5}} \tag{7}$$

The angle θ is often referred to as the Lode Angle.

Meridional Shape Parameters

To complete the definition of the shear failure surface given by Equation (1), this section next explains the definition of the meridional shape parameters a and b. As a bit of background these shape parameters can be thought of as best fitting the shear failure surface to laboratory data. The Ottosen model emphasizes simultaneous best fits to four types of laboratory data:

1. Unconfined compression strength, f_c' $\left(\theta = 60^\circ \text{ and } \cos 3\theta = -1\right)$.
2. Uniaxial tensile strength, f_t' $\left(\theta = 0^\circ \text{ and } \cos 3\theta = +1\right)$.
3. Biaxial compressive strength $\left(\sigma_1 = 0, \sigma_2 = \sigma_3 = \text{constant}, \theta = 0\right)$. In particular the constant stresses are set to $-1.16 f_c'$ corresponding to laboratory test of Kupfer et al. (1969,1973).
4. A triaxial compression state of stress $\left(\theta = 60^\circ\right)$ which gives the best fit to the data of Balmer (1949) and Richart et al. (1928). The specific point selected has nondimensional coordinates $\left(I_1 / \sqrt{3} f_c' \,,\, \sqrt{2J_2} \,/\, f_c'\right) = \left(-5 \,,\, 4\right)$.

The first three laboratory data points are fit exactly and the fourth point is used with a least squares algorithm to obtain a best fit.

In the Winfrith implementation of the Ottosen shear failure surface, the user is not allowed to determine the parameters a and b, but rather the parameters are internally generated based upon an undocumented data fit, and as mentioned above, the ratio of the unconfined tensile to compressive strengths.

The Winfrith model introduces the following three nondimensional constants[2]:

[2] These are labeled 'low pressure,' an alternative set for 'high pressure' is also provided in the source code but not used.

$$\begin{aligned}\alpha &= 1.16 \\ \beta &= 0.5907445 \\ \gamma &= -0.6123724\end{aligned} \tag{8}$$

These constants are used to evaluate the meridional shape parameters a and b:

$$\begin{aligned}b &= \frac{1 + R\alpha\frac{\gamma}{3} - \alpha^2\frac{\gamma}{3} - \frac{\alpha}{R}}{\alpha^2\frac{\beta}{3} - 3\alpha - R\alpha\frac{\beta}{3}} \\ a &= \beta b + \gamma\end{aligned} \tag{9}$$

Where $R = f_t' / f_c' < 1$ is the ratio of the unconfined tensile to compressive strengths.

Octahedral Shape Parameters

The remaining two parameters for this four parameter model are used to define the shape of shear failure surface in the octahedral (π-plane), and these are denoted as k_1 and k_2 in Ottosen's notation. Preliminary to defining these two parameters, the Winfrith model introduces two additional constants defined in terms of the above defined constants a and b:

$$\begin{aligned}c &= \frac{\sqrt{3}}{R}\left(1 - bR - R^2\frac{a}{3}\right) \\ d &= \frac{3 + 3b - a}{\sqrt{3}}\end{aligned} \tag{10}$$

Then the π-plane shape factors are defined as

$$\begin{aligned}k_2 &= \cos\left[3\tan^{-1}\left(\frac{1}{\sqrt{3}} - \frac{2d}{c\sqrt{3}}\right)\right] \\ k_1 &= \frac{c}{\cos\left[\frac{1}{3}\cos^{-1}\left(k_2\right)\right]}\end{aligned} \tag{11}$$

Equations (9) and (11) define the four parameters of the Ottosen shear failure surface.

The function $\lambda = \lambda\left(\cos 3\theta\right)$ is now defined in terms of the Lode Angle and the constants k_1 and k_2 as

$$\lambda = \begin{cases} k_1 \cos\left[\dfrac{\cos^{-1}\left(k_2 \cos 3\theta\right)}{3}\right] & \text{for } \cos 3\theta \geq 0 \\ k_1 \cos\left[\dfrac{\pi}{3} - \dfrac{\cos^{-1}\left(-k_2 \cos 3\theta\right)}{3}\right] & \text{for } \cos 3\theta \leq 0 \end{cases} \tag{12}$$

Plotting the shear failure surface in the octahedral plane, or π-plane or deviatoric plane, requires a bit more manipulation. In the previous section the meridional shapes of the shear failure surface were plotted by selecting fixed values of the angle θ, often referred to as the *similarity angle* $0 \leq \theta \leq \pi/3$, in particular $\theta = 0$ to generate the triaxial extension surface and $\theta = \pi/3$ to generate the triaxial compression surface. Note: additional surfaces could be drawn for all values of the similarity angle θ.

Octahedral planes are defined by constant values of I_1, or equivalently the mean stress. For such a constant I_1 value, the Ottosen shear failure surface, i.e. Equation (1) is only a function of the $\sqrt{J_2}$ and $\cos 3\theta$. These two parameters can conveniently be thought of as a radius and angle, respectively, in a polar type plot on a octahedral plane. The procedure is to select a value of the similarity angle θ and solve the for corresponding value of $\sqrt{J_2}$ from Equation (1) for the prescribed value of I_1, i.e. a particular octahedral plane. Then the Cartesian equivalent of polar coordinates are defined as

$$\begin{aligned} x &= r\cos\alpha \\ y &= r\sin\alpha \\ r &= \sqrt{2J_2} \\ 0 &\leq \alpha \leq 2\pi \end{aligned} \tag{13}$$

The angle α varies continuously to generate the polar plot and is related to the similarity angle via

$$\begin{aligned} \beta &= \frac{\sin^{-1}\left(\sin 3\alpha\right)}{3} \\ \theta &= \beta + \frac{\pi}{6} \end{aligned} \tag{14}$$

Here β is typically referred to as the Lode Angle and varies between $-\pi/6 \leq \beta \leq \pi/6$.

Figure 2 shows an illustration of the octahedral plane shape of the Ottosen shear failure surface. The value $I_1 = -6$ ksi (41 MPa) corresponds to a mean stress of -2 ksi $\left(= P = I_1/3\right)$ which is the constant mean stress plane that passes through the intersection of the shear failure surface with the unconfined compression stress trajectory, i.e. $SD = -3P = 6$ ksi $= f_c'$. Note: since the radius

used in the octahedral plane is $r = \sqrt{2J_2}$ that radius needs to be scaled by $\sqrt{3}/\sqrt{2} = 1.2247$ to determine the corresponding stress difference value for triaxial loading since $SD = \sqrt{3J_2}$. For example, the maximum triaxial compression value at the bottom of Figure 2 is 4898.98 x 1.2247 = 6000 psi = f_c'.

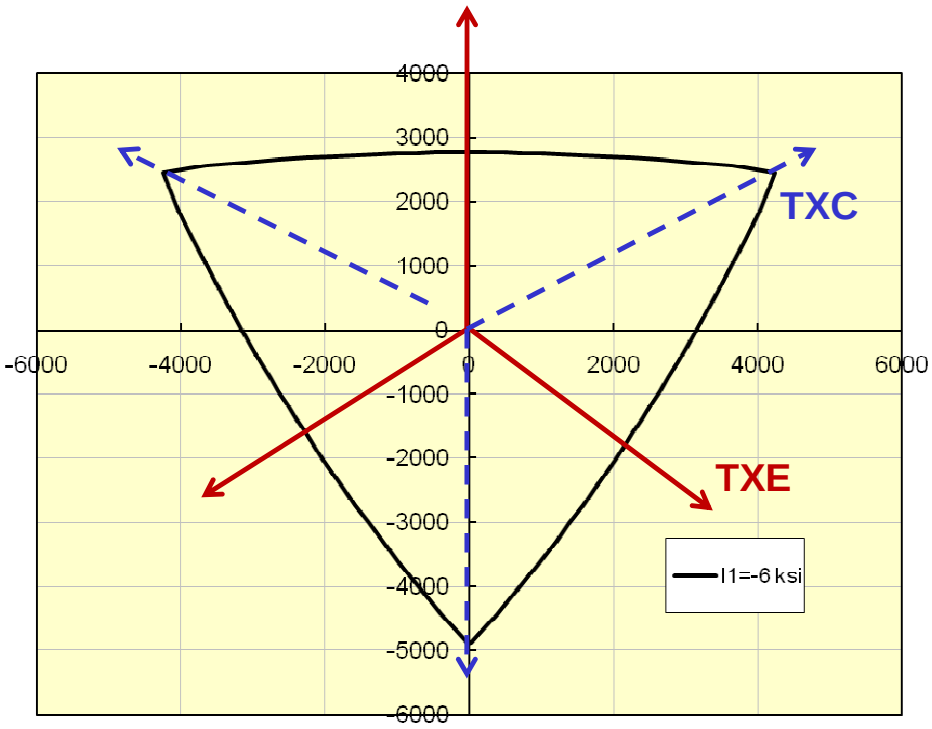

Figure 2 Illustration of the octahedral plane for a 6 ksi (41 MPa) unconfined compression strength concrete.

Pressure versus Volume Strain

The Winfrith concrete model is a so called 'flat cap' model in that in the meridional plane, i.e. $\left(I_1, \sqrt{J_2}\right)$, the pressure versus volume strain relation can be represented by a straight line normal to the mean stress axis. While the user may enter up to eight pairs[3] of natural volume strains and corresponding pressures, it is likely users will take advantage of the predefined pressure versus volume strain input option.

The first pair of points in the internally generated pressure versus volume strain is the strain and pressure that occur at the unconfined compression strength, f_c'. The mean stress is at this point is $P_c = f_c'/3$ and the volume strain is approximated as $\varepsilon_c^{vol} = P_c / K$ where the elastic bulk modulus is defined using the user input elastic modulus and Poisson's ratio, viz.

[3] Note: the origin point (0,0) may be omitted from the input as this point is treated internally in the Winfrith model.

$K = E/\left(3\left(1-2\nu\right)\right)$. Table 1 provides the ten pressure versus volume strain points generated by the Winfrith model.

Table 1 Winfrith concrete model generated pressure versus volume strain response.

Natural Volume Strain	Pressure (factor multiplies P_c)
$-P_c / K$	1.00
-0.002	1.50
-0.004	3.00
-0.010	4.80
-0.020	6.00
-0.030	7.50
-0.041	9.45
-0.051	11.55
-0.062	14.25
-0.094	25.05

Strain Rate Enhancement

A description of the Winfrith concrete model strain rate enhancement is provided by Broadhouse and Attwood (1993). This paper in turn cites a 1988 CEB Bulletin; the current CEB strain rate enhancement recommendation is provided in CEB (1990). The description presented in this section follows the present coding in the LS-DYNA Winfrith concrete model subroutine.

The strain rate enhancements are based upon the incremental strain rates

$$\dot{\varepsilon}_{ij} = \frac{\Delta\varepsilon_{ij}^{n}}{\Delta t} \tag{15}$$

Where $\Delta\varepsilon_{ij}^{n}$ is the current strain increment obtained from solving the equation of motion and Δt is the current time step. These incremental strain rates are used to form the incremental effective strain rate $\dot{e}$

$$\begin{aligned}
&\dot{\varepsilon}_{vol} = \dot{\varepsilon}_{kk} = \dot{\varepsilon}_{11} + \dot{\varepsilon}_{22} + \dot{\varepsilon}_{33} \\
&\dot{e}_{ij} = \dot{\varepsilon}_{ij} + \dot{\varepsilon}_{kk}\delta_{ij}/3 \\
&\dot{e} = \sqrt{\frac{2}{3}\dot{e}_{ij}\dot{e}_{ij}} = \sqrt{\frac{2}{3}\left[\dot{e}_{11}^2 + \dot{e}_{22}^2 + \dot{e}_{33}^2 + 0.5\left(\dot{e}_{12}^2 + \dot{e}_{23}^2 + \dot{e}_{31}^2\right)\right]}
\end{aligned} \tag{16}$$

If the incremental effective strain rate is less 30/second then ‘low’ strain rate factors are calculated, else if the incremental effective strain rate is greater than 30/second then ‘high’ strain rate factors are calculated.

For both the low and high strain rates, three strain rate enhancement factors are calculated: tensile E_T, compressive E_C, and Young's modulus E_E:

$$\begin{aligned} E_T &= \left(\frac{\dot{e}}{\dot{e}_{0T}}\right)^{1.016\delta} \qquad E_C = \left(\frac{\dot{e}}{\dot{e}_{0C}}\right)^{1.026\alpha} \qquad \dot{e} < 30/\mathrm{s} \\ E_T &= \eta \dot{e}^{1/3} \qquad E_C = \gamma \dot{e}^{1/3} \qquad \dot{e} > 30/\mathrm{s} \end{aligned} \tag{17}$$

Where

$$\begin{aligned} \delta &= \frac{1}{10 + 0.5 f_{cu}} \\ \alpha &= \frac{1}{5 + 0.75 f_{cu}} \\ \log_{10} \eta &= 6.933\delta - 0.492 \\ \log_{10} \gamma &= 6.156\alpha - 0.492 \\ \dot{e}_{0T} &= 30 \times 10^{-6}/\mathrm{s} \\ \dot{e}_{0C} &= 3 \times 10^{-6}/\mathrm{s} \end{aligned} \tag{18}$$

Here f_{cu} is the concrete cube strength in MPa. Note: concrete cubes rather than cylinders are typically used to determine the unconfined compressive strength in Europe. If f_c' is the cylinder unconfined compressive strength, then $f_{cu} = 1.25 f_c'$ is the corresponding cube strength. In the LS-DYNA implementation the user input uniaxial compressive strength is used as f_{cu}.

The Young's modulus rate enhancement is calculated as an average of tensile and compressive rate enhancements,

$$E_E = 0.5\left[\left(\frac{\dot{e}}{\dot{e}_{0T}}\right)^{0.016} + \left(\frac{\dot{e}}{\dot{e}_{0C}}\right)^{0.026}\right] \tag{19}$$

If any of the above rate enhancement factors are less than one, they are set equal to one, i.e. no rate enhancement.

The following material properties are then rate enhanced

Table 2 Material properties that are strain rate enhanced.

Material Property	Rate Enhancement Factor
Young's modulus	E_E
Shear modulus	E_E
Bulk modulus	E_E
f_c'	E_C
f_t'	E_T

Simple Loading Cases – Verification

In this section a few simple loading cases are simulated and the results compared with expected results: either as specified via input quantities or determined from the analytical form of the Winfrith concrete material model.

The input for the Winfrith material model, using the unit system of grams-millimeters-milliseconds (CONM=-3), is

```
$                                MPa - mm - msec
*MAT_WINFRITH_CONCRETE
$#     mid        ro        tm        pr       ucs       uts        fe     asize
        85   1.60e-3  33536.79       0.18     41.36     2.068     0.127     9.779
$#       e        ys        eh    uelong      rate      conm      conl      cont
                                                1.0      -3.0     0.000     0.000
$#    eps1      eps2      eps3      eps4      eps5      eps6      eps7      eps8
     0.000     0.000     0.000     0.000     0.000     0.000     0.000     0.000
$#      p1        p2        p3        p4        p5        p6        p7        p8
     0.000     0.000     0.000     0.000     0.000     0.000     0.000     0.000
```

This is a 41 MPa (6 ksi) unconfined compression strength concrete with a strength ratio of 0.05 $\left(= f_t'/\, f_c'\right)$, an approximate density of 2400 kg/m^3 (150 pcf), containing aggregate of 9.7 mm (0.385 inch) diameter, and specified to have a crack width dimension of 0.127 mm (0.005 inch) when no tensile force exists (controls the tensile softening response). Unless otherwise noted, the strain rate effects (RATE=1) are turned off.

Hydrostatic Compression Test

As described in the previous section, the Winfrith concrete model provides the user with a default pressure versus natural volume strain definition. A single solid hexahedra element, a unit cube, was used to verify the Winfrith default pressure versus volume strain response by prescribing uniform displacements on all side of the unit cube and plotting the resulting pressure versus natural volume strain, as shown in Figure 3. The solid line represents the continuous results from the LS-DYNA unit cube simulation and the filled squares are the Winfrith default pressure versus volume strain data from Table 1 for an unconfined compressive strength of 41

MPa and bulk modulus of 17.5 GPa. As can be seen in Figure 3, the LS-DYNA results reproduce the Winfrith default pressure versus volume strain data.

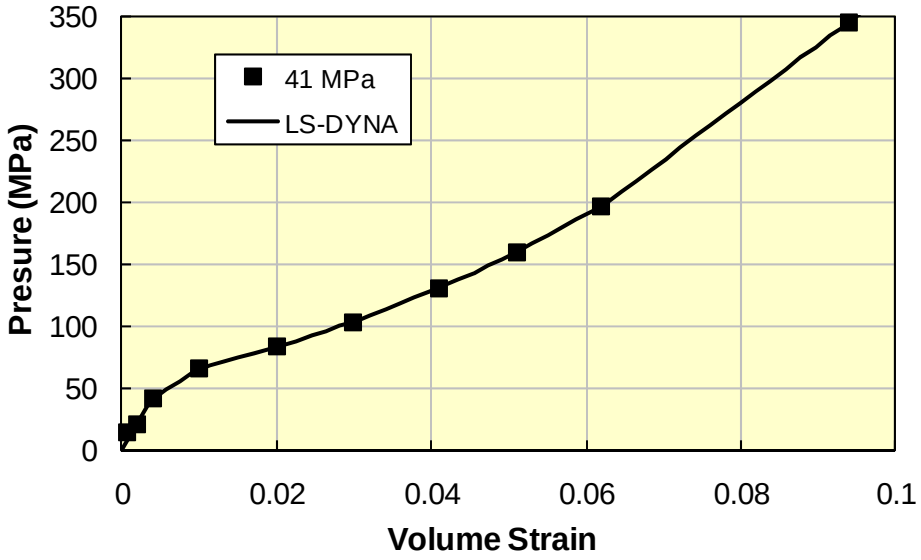

Figure 3 Verification of pressure versus volume strain for an f_c' =41 MPa concrete.

While such unit cube sample problems are easy to construct, it is recommended that more complex specimen geometries also be exercised. In particular, geometries with non-uniform mesh discretization to allow for the possibility of mesh sensitivities such as occur in softening or cracking response. Such a non-uniformly mesh of a right circular cylinder is shown in Figure 4. The cylinder has a diameter and height of 400 millimeters. Only half the cylinder is shown to indicating the 10 elements selected for sampling the various required stress and strain quantities.

Figure 5 shows that the LS-DYNA cylinder averaged pressure versus natural volume strain results also reproduce the Winfrith default pressure versus volume strain data, as expected.

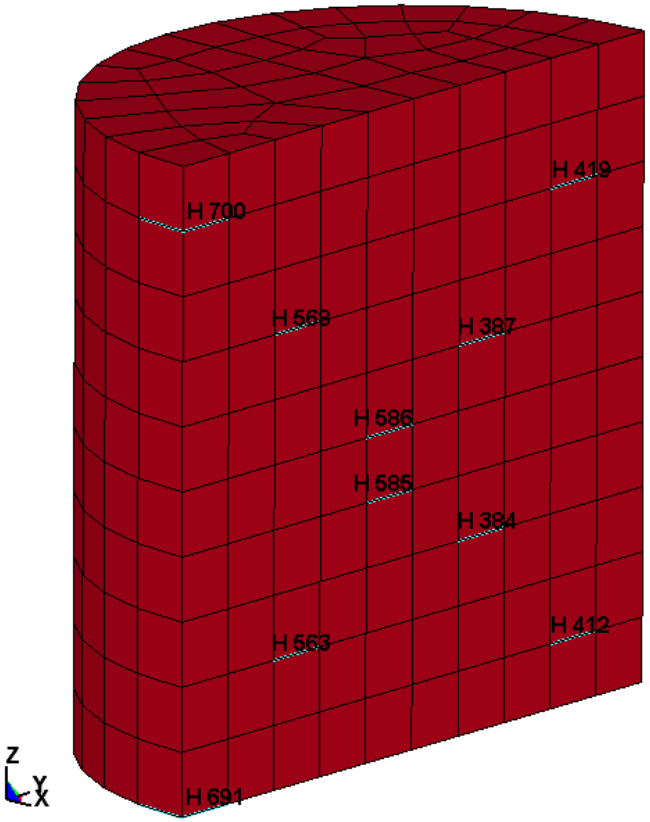

Figure 4 Non-uniformly meshed right circular cylinder.

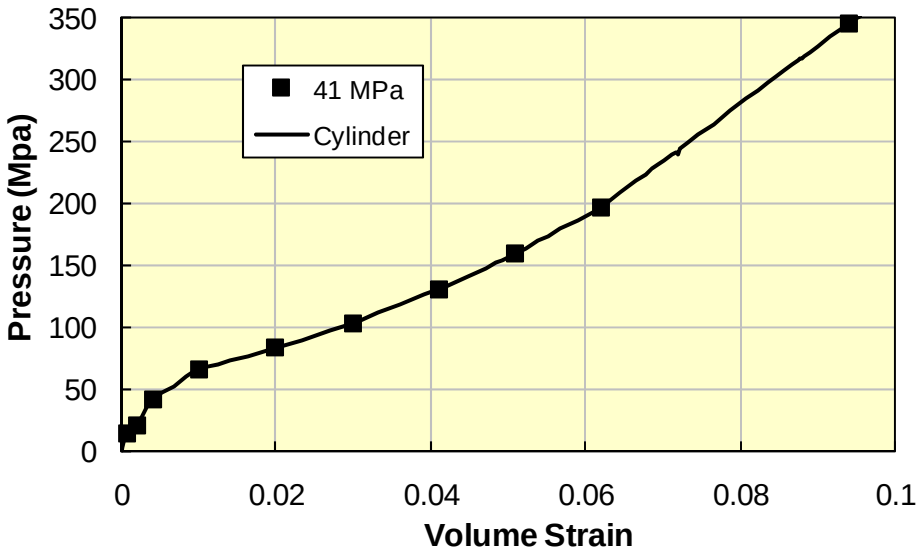

Figure 5 Verification of pressure versus volume strain for an f_c' =41 MPa concrete using the non-uniformly meshed cylinder.

Unconfined Compression Test

An unconfined compression test (UCT), see Figure 6, consists of a prescribed axial load on an otherwise unconstrained specimen. The laboratory version of this test is used to determine the unconfined compression strength f_c'.

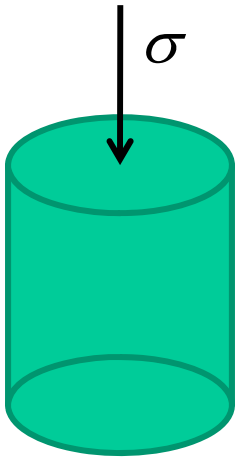

Figure 6 Schematic of an unconfined compression test.

Single Hexahedra

A single solid hexahedra element, a unit cube, was used to verify the prescribed unconfined compressive strength of 41.2 MPa. The boundary conditions consist of prescribed axial displacement on the top of the unit cube with the lateral surfaces traction free; the bottom surface is constrained against only axial motion.

Since this simulation is in a state of uniaxial stress, the axial strain at failure is given by

$$\varepsilon_{fail} = \frac{f_c'}{E} = \frac{41.2}{33536.8} = 1.22 \times 10^{-3} \tag{20}$$

The top surface was prescribed to move -0.002 mm at 1.5 ms (low strain rate of 1.3/second) and then remain constant, see Figure 7. For the unit cube specimen, this maximum displacement corresponds to an engineering axial strain of -0.002, which exceeds the failure strain. By exceeding the failure strain, via prescribed displacement, an assessment of possible strain softening in compression can be made.

Figure 8 shows the resulting axial stress versus axial strain for the unit cube unconfined compression test simulation; the geomechanics sign convention of compression positive is used in this figure. As expected, the unit cube does reach a maximum stress of 41.2 MPa at a strain of 0.00122. After this failure point the axial stress remains constant and the axial strain continues to

increase to the prescribed 0.002 value. There is no indication of strain softening in this simulation.

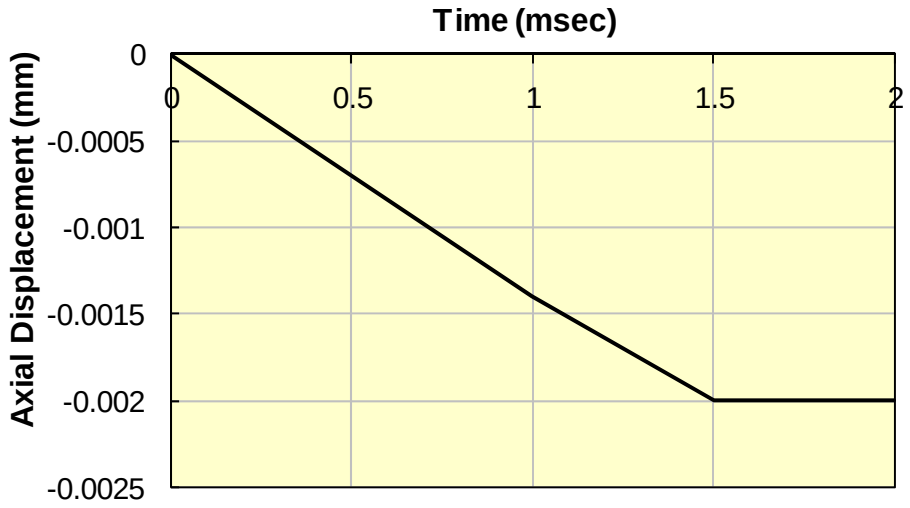

Figure 7 Prescribed axial displacement for top surface in unconfined compression simulation.

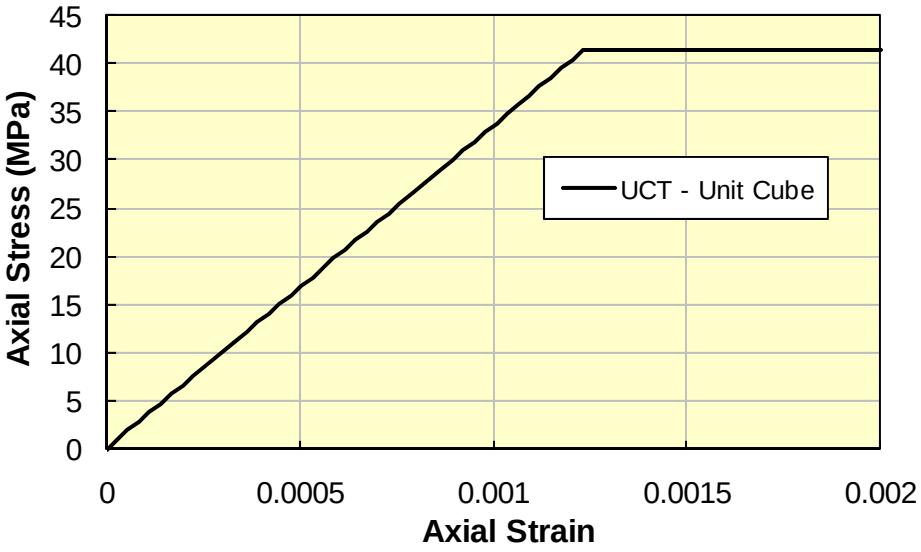

Figure 8 Axial stress versus axial strain for unit cube UCT simulation.

Figure 9 shows the axial and lateral strain histories from the unit cube unconfined compression test simulation. In this figure there is a change in the slope of the lateral strain at about 0.9 ms which corresponds to the time when the axial failure strain of 0.00122 is attained. At this point two orthogonal crack planes are introduced by the Winfrith concrete model, as shown in Figure 10. These orthogonal crack planes are oriented parallel to the compression direction. Although the axial strain ceases to increase after 1.5 ms, as prescribed, the lateral strains continue to

increase as the lateral momentum imparted to the nodes, via the Poisson effect, continues to move these nodes at a constant lateral velocity, since the element has no stress in the lateral direction; recall the element was traction free on the lateral surface, e.g. zero lateral stress.

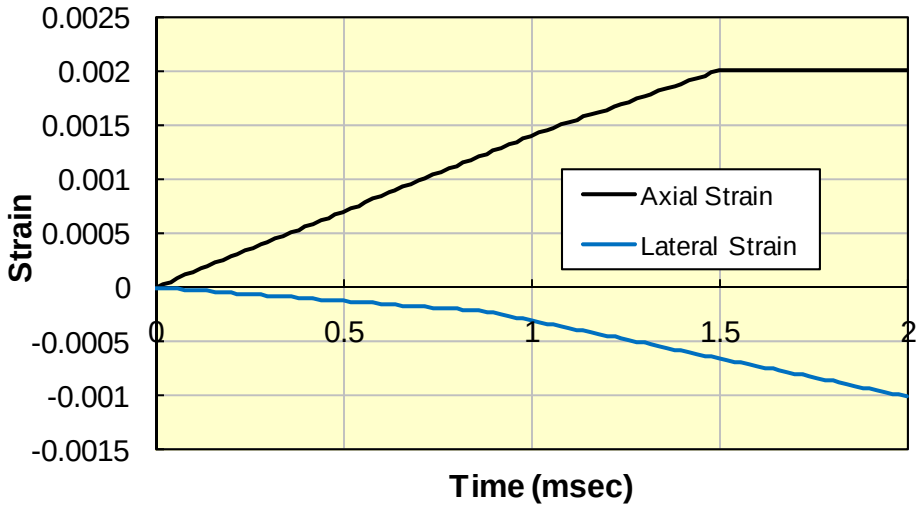

Figure 9 Axial and lateral strain histories for unit cube simulation of an unconfined compression test.

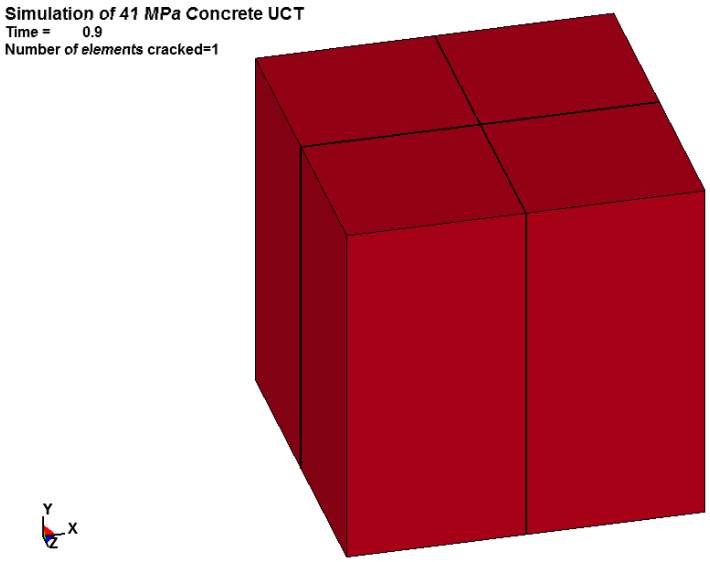

Figure 10 Two orthogonal crack planes introduced in the unit cube when the unconfined compressive strength is reached.

Non-uniformly Meshed Cylinder

The same unconfined compression test simulation is performed using the non-uniformly meshed right circular cylinder. Again the boundary conditions are prescribed displacement of the top

surface and traction free lateral surfaces. The top surface displacement is prescribed to move 0.488 mm in 15 ms, for an engineering axial strain of 0.00122, since the cylinder is 400 mm in length. After this compressive failure strain is reached, the top surface continues to a prescribed displacement of 0.8 mm at 20 ms, and then the displacement is held constant. This is a lower strain rate of 0.1/second than used in the unit cube (1.3/second) since that faster strain rate does not approximate quasi-static response in the cylinder, i.e. wave propagation effects will be present.

Figure 11 shows a comparison of the axial stress versus axial strain from the unit cube and the non-uniformly meshed cylinder. As expected, the axial stress strain response for the unit cube and cylinder are nearly identical. For the cylinder, an average of the axial stress and strain from the 10 selected (refer back to Figure 4) elements was used in constructing the stress-strain response. The amount of *lateral strain* variability in the 10 elements selected from the cylindrical sample is shown in Figure 12.

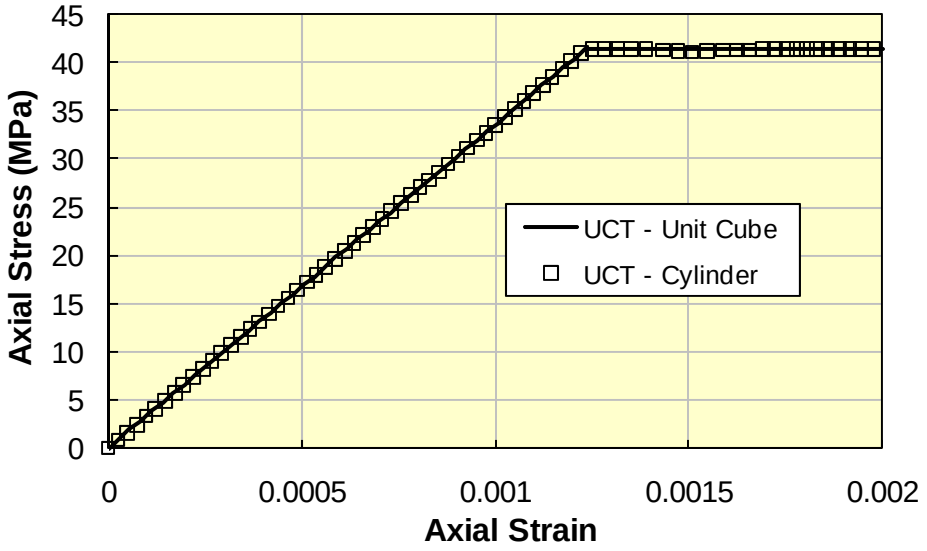

Figure 11 Comparison of unit cube and cylinder axial stress versus axial strain for UCT simulation.

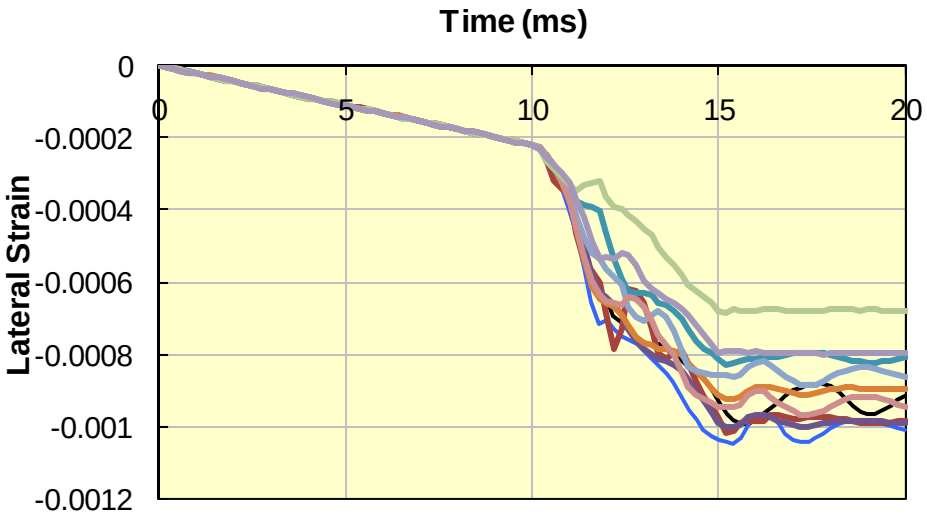

Figure 12 Illustration of variability in the lateral strains for the 10 selected elements of the non-uniformly meshed cylinder.

Figure 13 compares the unit cube and averaged axial and lateral strain histories obtained from the non-uniformly mesh cylinder; again the geomechanics sign convention of compression positive has been used. Note: the lateral strains for the cylinder were obtained by requesting the maximum principal strains from the post-processor. The slight difference in slope during the elastic portion of the simulation is due to the two different strain rates. Of interest is the different response for the lateral strains from the cylinder. These strains remain constant while the top surface displacement is constant. This is in contrast to the unit cube, which due to complete failure, continues to strain in the lateral direction due to the imparted lateral momentum.

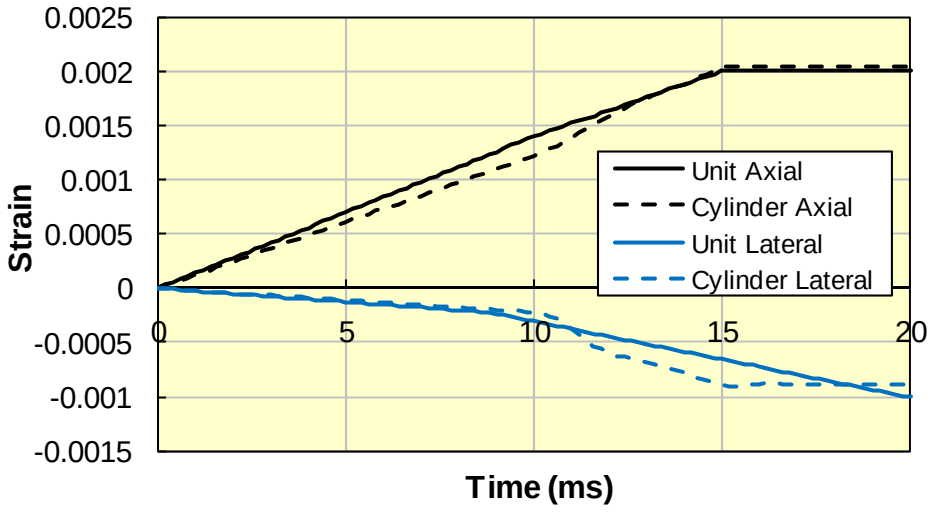

Figure 13 Averaged axial and lateral strain histories from unit cube and non-uniformly meshed cylinder.

The cracking of the non-uniformly meshed cylinder is shown in Figure 14. This figure indicates that not all the elements of the cylinder are cracked, and in particular the cracks do not extend the full height of the cylinder in some axial columns of elements. Since some elements are not fully cracked, the cylinder can resist lateral motion, due to Poisson induced inertial effects, and hence the average lateral strains, shown previously in Figure 13, remain constant when the loading does not increase.

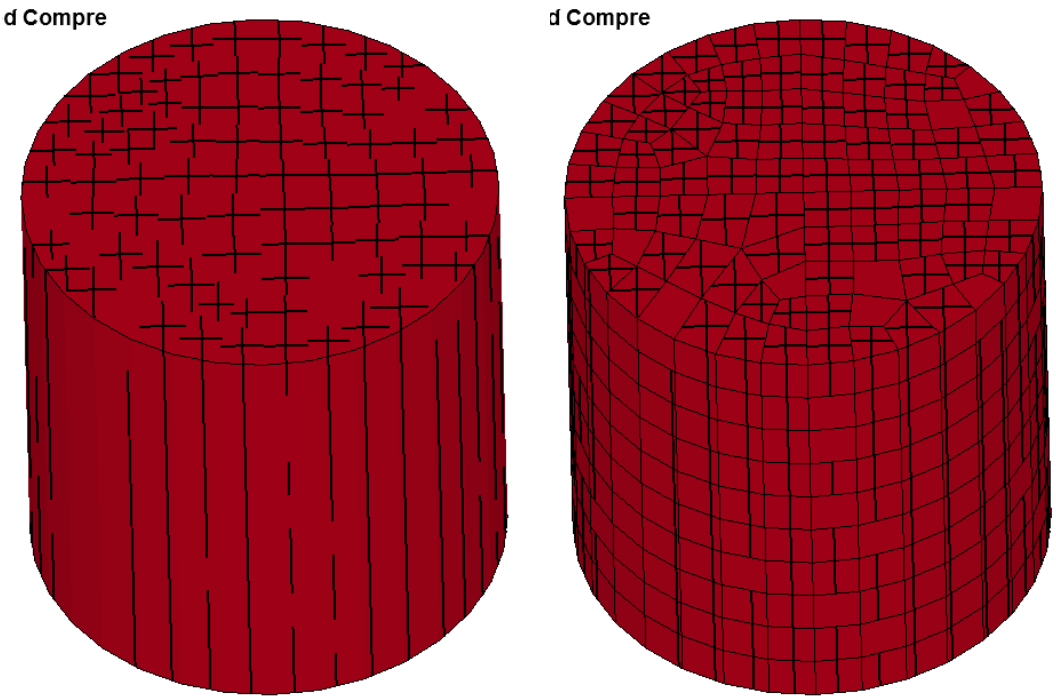

Figure 14 Winfrith crack pattern for non-uniformly meshed cylinder without (left) and with (right) element mesh overlay.

Uniaxial Tension Test

The uniaxial tension test (UTT), see Figure 15, consists of a prescribed axial load on an otherwise unconstrained specimen. The laboratory version of this test is used to determine the unconfined compression strength f_t'.

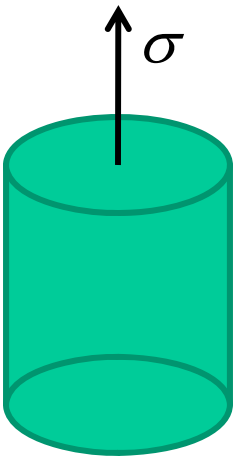

Figure 15 Schematic of an uniaxial tension test.

Single Hexahedra

A single solid hexahedra element, a unit cube, was used to verify the prescribed uniaxial tensile strength of 2.068 MPa. The boundary conditions consist of prescribed axial displacements on the top of the unit cube with the lateral surfaces traction free.

Since this simulation is in a state of uniaxial stress, the axial strain at failure is given by

$$\varepsilon_{fail} = \frac{f_t'}{E} = \frac{2.068}{33536.8} = 6.16 \times 10^{-5} \tag{21}$$

Although this is the strain at which failure is *initiated*, the failure is not complete until the crack width has attained the prescribed width at which the stress goes to zero, i.e. the Winfrith input parameter FE=0.127 mm.

The top surface was prescribed to move 0.15 mm at 10 ms (low strain rate of 15/second), then remain constant until 20 ms, returning to zero at 30 ms, and then into compression with -0.15 mm displacement at 40 ms, see Figure 16. For the unit cube specimen, this maximum tensile displacement corresponds to an engineering axial strain of 0.15, which exceeds the tensile failure initiation strain and the corresponding crack width (strain) at failure of 0.127 mm. By exceeding the failure initiation and crack width strains, via prescribed displacement, an assessment of the strain softening in tension can be made.

Also, reversing the tensile strain and ‘healing’ the crack allows an assessment of the cracked element’s ability to carry subsequent compression.

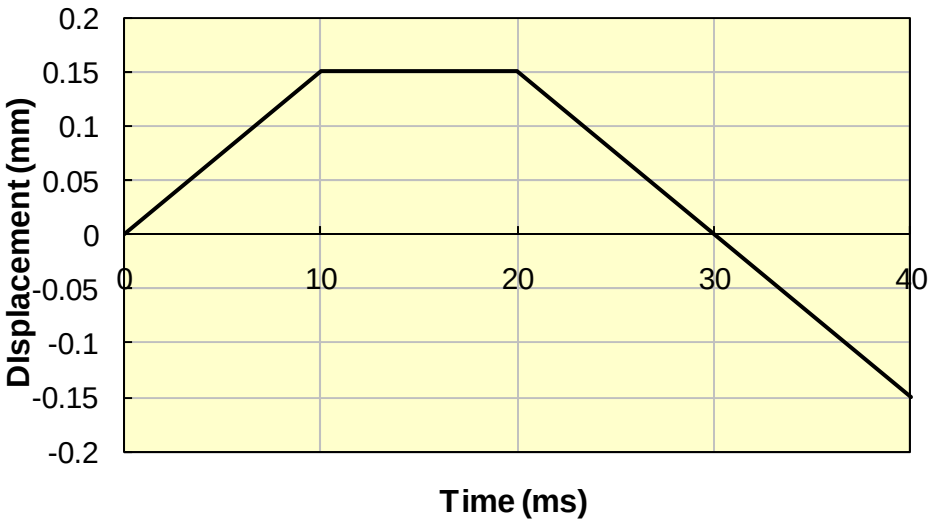

Figure 16 Prescribed axial displacement for top surface in uniaxial tension/compression simulation.

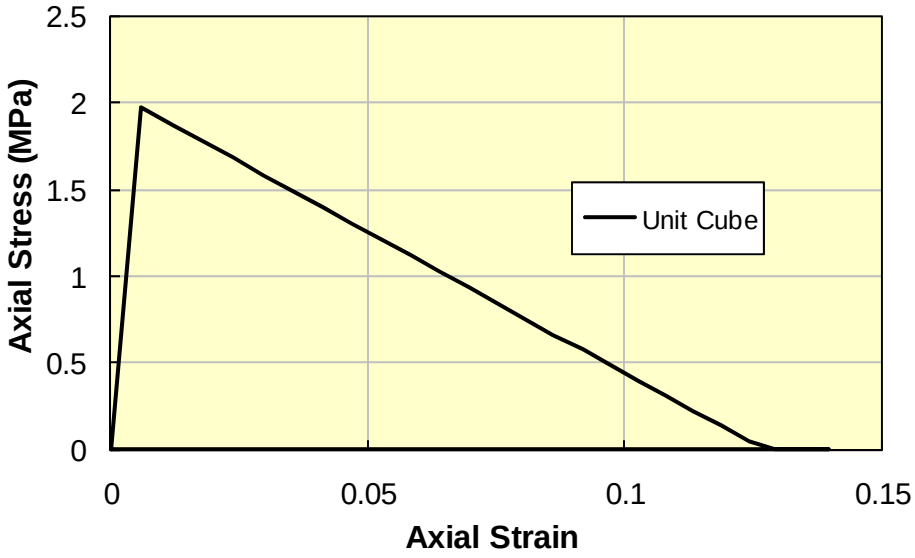

Figure 17 Axial stress versus axial strain for unit cube UTT simulation.

Figure 17 shows the axial stress versus axial strain from the tensile portion of the unit cube uniaxial tensile/compression simulation. As expected, the maximum stress of 2.068 MPa was reached at an axial strain of 1.66×10^{-5}; Figure 17 depicts the maximum stress of 1.97 MPa at a strain of 5.98×10^{-3} as those were the values with the minimum sampling rate of 0.4 ms. The maximum stress then decreases linearly to a strain of 0.127 which corresponds to the Winfrith parameters FE=0.127 mm. The prescribed axial strain then increases to 0.15 before reversing and returning to zero strain.

Next the strain is increased in compression from the zero value at the end of the tensile cycle to a compressive strain of -0.15. The correspond axial stress versus axial strain is shown in Figure 18. The complete axial stress strain cycle is shown in Figure 19.

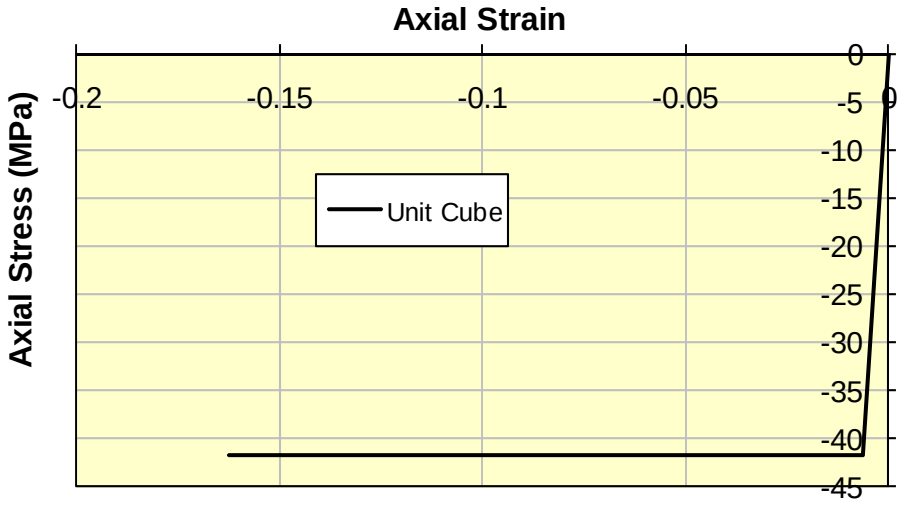

Figure 18 Axial stress versus axial strain for compressive loading following tensile failure.

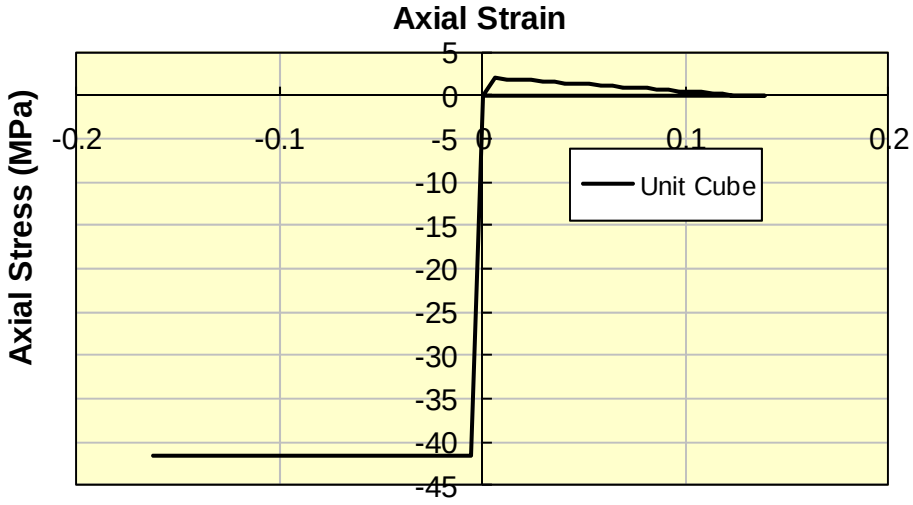

Figure 19 Complete axial stress versus axial strain response for uniaxial tensile and compressive cycle of loading.

Figure 20 shows the single crack plane that develops in the unit cube when the crack width displacement criterion is satisfied, i.e. FE=0127 mm at 9.2 ms. The crack plane is perpendicular to the (vertical) loading direction. Subsequently, at 30.4 ms, in the compression portion of the loading cycle, this horizontal tension crack plane is 'healed' and a pair of orthogonal crack planes develops when the unconfined compression strength is reached.

Figure 20 Single tensile crack plane introduced in unit cube when the uniaxial tensile strength is reached (left) and double orthogonal tensile crack planes when compressive strength is reached.

Non-uniformly Meshed Cylinder

The same cyclic uniaxial test simulation is performed using the non-uniformly meshed right circular cylinder. Again the boundary conditions are prescribed displacement of the top surface and traction free lateral surfaces. The top surface displacement is prescribed to move 0.15 mm in 15 ms, for an overall average engineering axial strain of 3.75×10^{-4}, since the cylinder is 400 mm in length. However, since there are 10 elements along the 400 mm cylinder height, the nominal element strain would be $3.75\times10^{-5}\left(=3.75\times10^{-4}/10\right)$. While both of these strains exceed the initial failure strain of 6.16×10^{-5}, the equivalent strain at which the crack stress is zero would be $3.175\times10^{-4}\left(=0.127/400\right)$ for overall specimen average, or $3.175\times10^{-5}\left(=3.175\times10^{-4}/10\right)$ for a nominal element. If the equivalent strain at which the crack stress is zero, localizes in one element, then the strain will be $3.175\times10^{-3}\left(=0.127/40\right)$, i.e. all the displacement will occur in one element.

As with the unit cube, once the top surface reached the prescribed displacement of 0.15 mm at 15 ms, then the displacement is held constant until 20 ms when it is reduced back down to zero. This completes the tension portion of the loading cycle. Next the strain is increased in compression with a top surface moving to -0.55 mm at 40 ms, see Figure 21. The 0.55 mm compressive displacement provides an average compressive strain of 1.375×10^{-3} which exceeds the compressive failure strain of 1.22×10^{-3}, recall Equation (20). Again the intent of the strain reversal is to make an assessment of the cylinder's ability to carry compression after tensile failure.

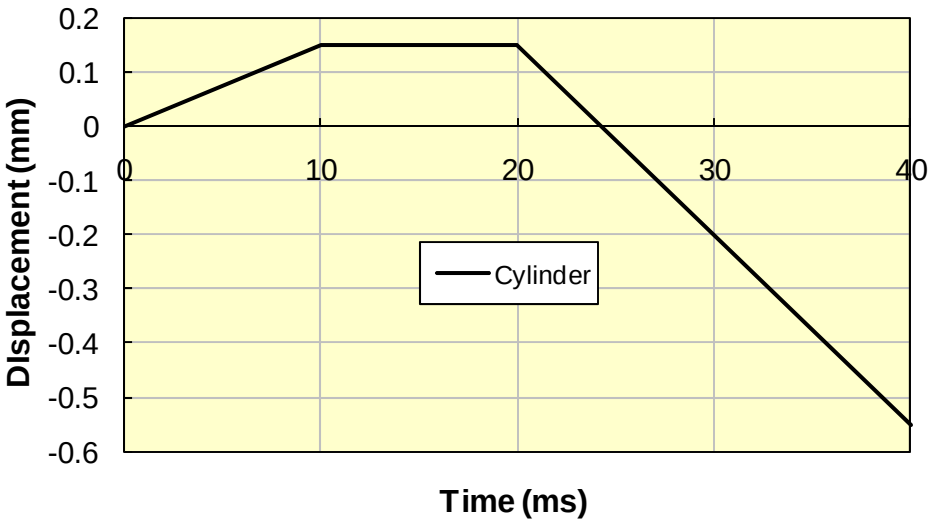

Figure 21 Tension and compression loading cycle for the non-uniformly meshed cylinder.

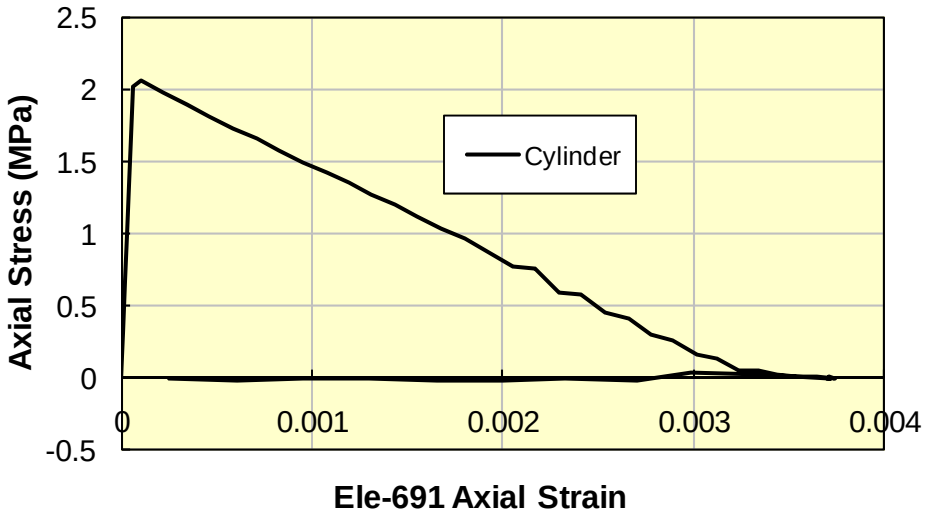

Figure 22 Axial stress versus Element 691 axial strain for cylinder UTT simulation.

Figure 22 shows the axial stress versus axial strain (Element 691) for the non-uniformly meshed cylinder acting under the uniaxial tension portion of the above described loading. The reason for plotting the axial strain for Element 691, rather than the average axial strain, is the displacement localized in the bottom layer of the cylinder's elements, where Element 691 is located. Figure 23 shows the Winfrith model tensile cracks and the location of Element 691. Since the Winfrith model cracks localized in one layer of the cylinder, the other elements in the cylinder had very low strain levels, i.e. up to the initial failure strain (elastic response), and then these low strain levels decreased to zero as the bottom layer of elements in the cylinder accounted for all the overall strain via localization.

Next the strain is increased in compression from the zero value at the end of the tensile cycle to a compressive strain of 1.375×10^{-3} which exceeds the compressive failure strain. The correspond axial stress versus axial strain is shown in Figure 24. The complete axial stress strain cycle is shown in Figure 25.

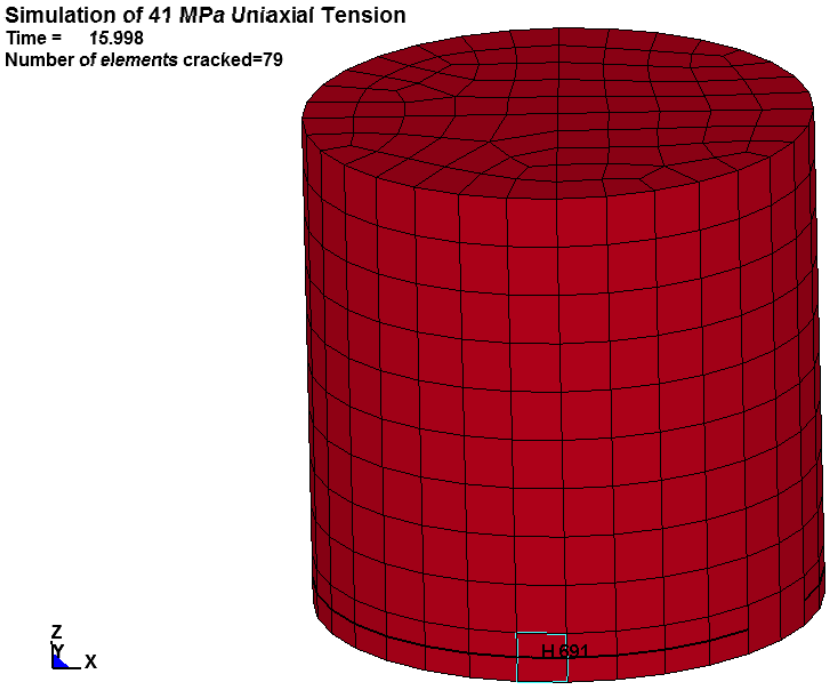

Figure 23 Winfrith model crack pattern at bottom layer of non-uniformly meshed cylinder for UTT simulation.

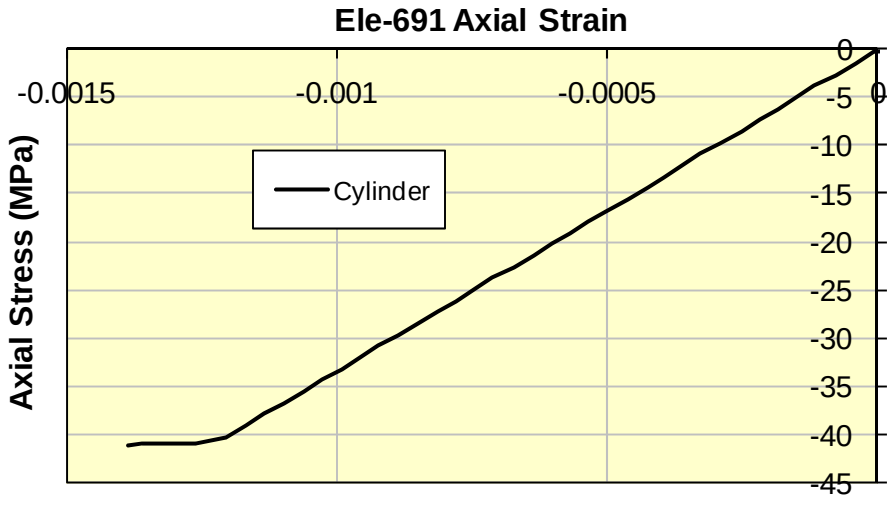

Figure 24 Axial stress versus axial strain for compressive loading following tensile failure in the cylinder model.

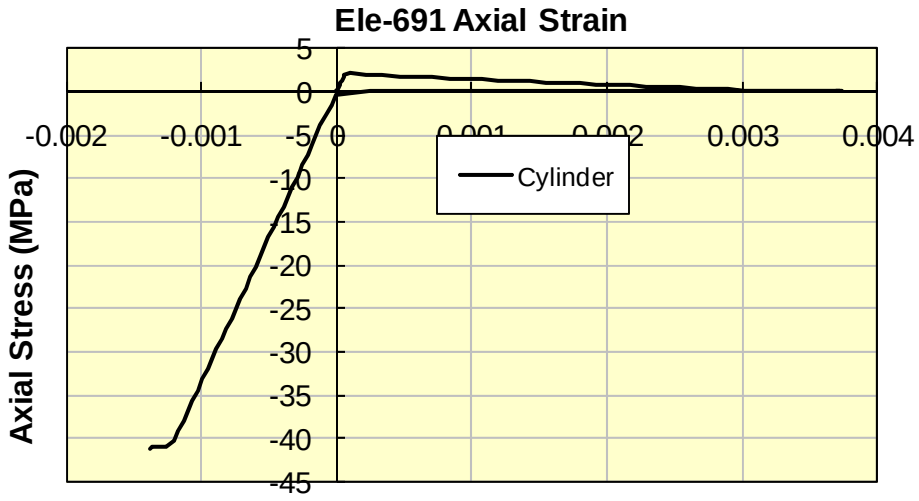

Figure 25 Complete axial stress versus axial strain response for uniaxial tensile and compressive cycle of loading for the non-uniformly meshed cylinder.

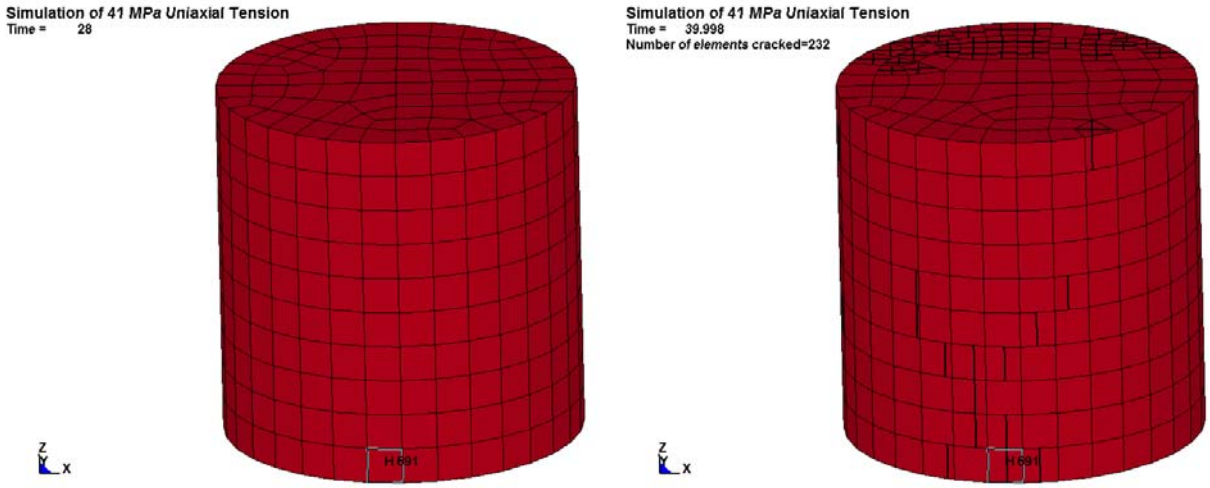

Figure 26 Healed tension crack (left) a 29 ms and appearance of compressive orthogonal crack planes at 40 ms (right).

Figure 26 shows the 'healing' of the Winfrith concrete model tension cracks in the bottom layer of the cylinder at 28 ms. As the compressive portion of the loading cycle continues, pairs of orthogonal tension cracks develop when the compressive failure strain is reached at 40 ms.

It is observed that this crack pattern due to compression after a tension failure cycle is quite different from that obtained for the compression only (unconfined compression tests) simulation, see previous Figure 14.

Simple Loading Cases - Conclusions

The specified compressive and tensile failure strengths and strains were verified via these simple loading cases.

In unconfined compression, the unit cube developed an orthogonal set of Winfrith concrete model crack planes, which are aligned with the compression direction, see Figure 10. It was noted that there is no strain softening after the compression failure occurs. The unconfined compression strength was maintained while the axial and lateral strains increased, i.e. elastic perfectly plastic behavior. While behavior similar to the unit cube was observed for the non-uniformly mesh cylinder, Winfrith concrete model crack planes that develop did not occur in all elements comprising the cylinder. This indicates a mesh size sensitivity.

In the uniaxial tension and compression cyclic loading, the unit cube developed a single Winfrith concrete model tensile crack plane perpendicular to the tensile loading direction. During the subsequent compression portion of the cyclic loading, the tensile crack is healed, the unit cube carries compression until the compressive failure strain is reached when the orthogonal set of Winfrith concrete model crack planes, aligned with the compression direction, develop.

The corresponding behavior for the non-uniformly mesh cylinder demonstrated an apparent lack of strain softening regularization as the Winfrith concrete model tensile crack plane developed only in the bottom layer of elements, and not all those elements were cracked. Further studies of this apparent lack of regularization are recommended, e.g. a rod of solid elements with varying dimensions under tensile loading can be used to assess if the tensile strain always localizes in the smallest element. During the compressive portion of the cyclic loading, the tensile cracks were again ‘healed,’ and subsequently orthogonal pairs of Winfrith concrete model planes developed when the compressive failure strain was reached. Oddly, the Winfrith concrete model crack pattern for this compressive loading is quite different than the corresponding crack pattern for the unconfined compression only simulation.

Acknowledgement

The help and guidance of Richard Sturt and Conrad Izatt, both of ARUP UK, is most greatly appreciated in navigating many aspects of the Winfrith concrete model.

References

Balmer, G.G. (1949) “Shearing strength of concrete under high triaxial stress - computation of Nohrs envelope as a curve,” United States Department of the Interior. Bureau of Reclamation. Structural Research Laboratory. Report No.SP-23, page 13.

Broadhouse, B.J. and G.J. Attwood (1993), “Finite Element Analysis of the Impact Response of Reinforced Concrete Structures using DYNA3D.” Proceedings of Structural Mechanics in Reactor Technology (SMiRT) 12, University of Stuttgart Germany Elsevier Science Publishing.

Kupfer, H., Hilsdorf, H.K. and Rosch, H. (1969) “Behaviour of Concrete under Biaxial Stresses,” *Proceedings of the American Concrete Institute*, Volume 66, pages 656-666.

Kupfer, H. and Gerstle, K. (1973) “Behaviour of Concrete under Biaxial Stress,” *Journal of the Engineering Mechanics Division*, American Society of Civil Engineers, Volume 99, pages 852-866.

Ottosen, N.S., (1977) “A Failure Criterion for Concrete,” *Journal of the Engineering Mechanics Division*, Volume 103, Number 4, July/August, pages 527-535.

Richart, F.E., Braendtzaeg, A., and Brown, R.L. (1928) “A Study of the Failure of Concrete under Combined Compressive Stress,” University of Illinois. Engineering Experimental Station. Bulletin Number 185, page 103.

Malvern, L.E. (1969), *Introduction to the Mechanics of a Continuous Medium*, Prentice-Hall, Englewood Cliffs, NJ.

Spiegel, M.R., (1968) *Schaum's Outline of Mathematical Handbook of Formulas and Tables*, McGraw-Hill Inc., New York, NY.

Comite Euro-International du Beton, *CEB-FIP model code 1990*, Redwood Books, Trowbridge, Wiltshire, UK, 1993.

CEB Bulletin Number 187 (1988), *Concrete Structures under impact and Impulsive Loading - Synthesis Report.*